Blind Symbol Rate Estimation of Faster-than-Nyquist Signals Based on Higher-Order Statistics

Albert Abelló[1,2], Damien Roque[2], and Jean-Marie Freixe[1]

[1] Eutelsat S.A., Paris, France.
aabellob@eutelsat.com
[2] Institut Supérieur de l'Aéronautique et de l'Espace (ISAE-SUPAERO), Université de Toulouse, Toulouse, France.

Abstract. Both faster-than-Nyquist (FTN) and cognitive radio go towards an efficient use of spectrum in radio communications systems at the cost of an added computational complexity at the receiver side. To gain the maximum potential from these techniques, non-data-aided receivers are of interest. In this paper, we use fourth-order statistics to perform blind symbol rate estimation of FTN signals. The estimator shows good performance results for moderate system's densities beyond the Nyquist rate and for a reasonable number of received samples.

Key words: blind symbol rate estimation, spectrum sensing, faster-than-Nyquist signaling, cyclostationary signals, higher-order statistics.

1 Introduction

Cognitive radio (CR) is primarily intended to improve the utilization of the radio electromagnetic spectrum [8]. To this end, a CR system can be basically described by a two-step process: (i) radio scene analysis (*i.e.*, detection of spectrum holes, estimation of the signal-to-interference-plus-noise ratio...) and (ii) selection and operation of an appropriate waveform (*i.e.*, channel estimation, transmit power control...). Among the constraints to be fulfilled by the chosen waveform, flexibility and spectral efficiency are found at the top of the list [2].

In the past decades, radio transmission systems were tied to the Nyquist criterion to ensure perfect reconstruction of the symbols with the help of linear systems. The symbol rate was thus bounded by the bilateral bandwidth of the transmitted signal and the only way to increase the spectral efficiency was to increase the constellation size. Even if significant improvements in the receivers sensitivity justify this approach, one may still wonder if the Nyquist criterion is a necessary condition for reliable transmission of information.

The idea of "faster-than-Nyquist" (FTN) signaling was first developed by J.E. Mazo [11] in 1975: the symbol rate is increased such that interpulse interference cannot be cancelled by linear filtering at the receiver side. However, FTN systems operating below the Mazo limit may preserve similar performance

to that of Nyquist systems, at the cost of non-linear processing [6]. Unfortunately, the additional algorithmic complexity induced has delayed the implementation of FTN systems for several decades. Iterative equalization and decoding techniques [5, 19] combined with increasing computational capabilities have renewed the interest in FTN signaling, enabling spectral efficiency gains up to 8-20 % [12, 15, 14, 10, 1].

In most applications, pilots and preambles are usually inserted to assist synchronization in receivers. However, it is preferable not to send these helper elements to preserve the spectral efficiency brought by FTN. It is thus desirable to perform non-data-aided (*i.e.*, blind) spectrum sensing, synchronization, channel estimation... However, FTN signaling rises several challenges due to the absence of second-order cyclic-correlation features, as it will be shown in the following. In particular, state of the art signal detection and blind symbol rate estimation techniques using second-order cyclostationarity do not apply in the FTN case [9, 18, 13].

In this paper, we show that a fourth-order extension of the symbol rate estimator presented in [4] is required to operate on FTN signals. We discuss the performance of our estimator in terms of dynamic range with respect to several parameters such as the transmission density or the number of received symbols.

The paper is organized as follows. Section 2 first defines a single-carrier FTN signal model and analyzes the conditions under which higher-order cylostationary features are present. Secondly, a blind symbol rate estimator for FTN signals is proposed using the reduced-dimension cyclic temporal moment function. Section 3 discusses the performance of the proposed estimator by means of simulations over an additive white Gaussian noise (AWGN) channel. Concluding remarks and insights are presented in Section 4.

2 System model: single-carrier linear transmitter

2.1 Faster-than-Nyquist signaling

Let $\{c_k\}_{k\in\mathbb{Z}}$ be a square summable sequence of independent and identically distributed (IID) symbols to be transmitted. Each complex symbol c_k is taken in a constellation $\mathbb{A}$. The complex baseband signal at the output of the transmitter is obtained by associating each c_k with a pulse shape $h(t) \in \mathbb{C}$ of finite energy

$$s(t) = \sum_{k=-\infty}^{\infty} c_k \, h(t - kT_s), \quad t \in \mathbb{R} \tag{1}$$

with T_s the elementary symbol spacing.

For this system, we can define the transmission density as $\rho = 1/(T_s B)$ where B is the transmitted signal bandwidth (assumed finite). Based on the frame theory [3, Ch. 7], one can note that:

– if $\rho \leq 1$, perfect symbol recovery can be obtained using a linear receiver;

– if $\rho > 1$, inter-symbol interference unconditionally appears at the output of a linear receiver, but symbols may still be recovered by using a nonlinear post-processing, knowing the initial constellation [6].

The former category includes traditional Nyquist systems while the latter defines FTN systems throughout this paper.

2.2 Higher-order statistics of FTN signals

The nth-order statistical moment of the transmitted signal is given by [7]

$$\begin{aligned} R_s(t,\boldsymbol{\tau})_n &= \mathrm{E}\left\{\prod_{i=1}^{n} s^{(*)i}(t+\tau_i)\right\} = \mathrm{E}\left\{\prod_{i=1}^{n}\sum_{k=-\infty}^{\infty} c_k^{(*)i} h^{(*)i}(t-kT_s+\tau_i)\right\} \\ &= \sum_{k_1\in\mathbb{Z}}\cdots\sum_{k_n\in\mathbb{Z}} \mathrm{E}\left\{c_{k_1}^{(*)1}\dots c_{k_n}^{(*)n}\right\} h^{(*)1}(t-k_1T_s+\tau_1)\dots h^{(*)n}(t-k_nT_s+\tau_n) \end{aligned} \tag{2}$$

where $(\cdot)^{(*)i}$ indicates an optional conjugation on the ith factor and $\boldsymbol{\tau} = [\tau_1,\dots,\tau_n]^T$, with $(\cdot)^T$ the transpose operator. In the following, we consider any conjugation set that allows the expectation in (2) being non-zero for some combination $k_1,\dots,k_n$. A discussion on this choice can be found in [16]. The second and higher-order moment function of a linearly modulated signal has been widely described in [17]. One remarks from (2) that $R_s(t+T_s,\boldsymbol{\tau})_n = R_s(t,\boldsymbol{\tau})_n$. We consider that $R_s(t,\boldsymbol{\tau})_n$ is absolutely integrable over a period T_s so that we can develop the Fourier series with coefficients

$$R_s^{\alpha}(\boldsymbol{\tau})_n = \frac{1}{T_s}\int_{-T_s/2}^{T_s/2} R_s(t,\boldsymbol{\tau})_n e^{-j2\pi\alpha t}\mathrm{d}t \tag{3}$$

where α denotes the cyclic frequency which may be non-zero for particular values $p/T_s, p\in\mathbb{Z}$. The expression in (3) is commonly referred to as the cyclic temporal moment function (CTMF). The transmitted signal is said nth order cyclostationary if there exists some non-zero α such that (3) is non-zero. To prove that higher-order cyclostationary features are present in FTN signals, let us consider the case $k_1 = k_2 = \dots = k_n = k$ yielding

$$R_s(t,\boldsymbol{\tau})_n = R_{c,n}\sum_{k=-\infty}^{\infty}\prod_{i=1}^{n} h^{(*)i}(t-kT_s+\tau_i) \tag{4}$$

where we define $R_{c,n} = \mathrm{E}\{|c_k|^n\}$ assumed non-zero in the following. Without loss of generality and for the sake of simplicity, we consider here the reduced-dimension cyclic temporal moment function (RD-CTMF) by setting $\tau_n = 0$.

$$\begin{aligned} R_s^{\alpha}(\boldsymbol{\tau}')_n &= \frac{1}{T_s}\int_{-T_s/2}^{T_s/2} R_s(t,\boldsymbol{\tau}')_n e^{-j2\pi\alpha t}\mathrm{d}t \\ &= \frac{R_{c,n}}{T_s}\int_{-\infty}^{\infty} h^{(*)n}(t)\prod_{i=1}^{n-1} h^{(*)i}(t+\tau_i)e^{-j2\pi\alpha t}\mathrm{d}t \end{aligned} \tag{5}$$

where $\boldsymbol{\tau'} = [\tau_1, \ldots, \tau_{n-1}]^T$, are the reduced-dimension time lags. Since linearly modulated signals considered here are assumed bandlimited, a frequency representation of the RD-CTMF is of interest. To this extent, we introduce the reduced-dimension cyclic spectral moment function (RD-CSMF):

$$S_s^{\alpha}(\boldsymbol{f'})_n = \int_{\boldsymbol{\tau'}} R_s^{\alpha}(\boldsymbol{\tau'})_n \, e^{-j2\pi \boldsymbol{f'}^T \boldsymbol{\tau'}} \mathrm{d}\boldsymbol{\tau'} \tag{6}$$

where $\boldsymbol{f'} = [f_1, \ldots, f_{n-1}]^T$ are the reduced-dimension frequency lags. Let us define $\mathbf{1} = [1, \ldots, 1]^T$ the indicator column vector function of size $n-1$. For the sake of notation simplicity, we consider in the following that the pulse shape takes values in the real field (*i.e.*, $h(t) \in \mathbb{R}$). It can be then shown [17] that

$$S_s^{\alpha}(\boldsymbol{f'})_n = \frac{R_{c,n}}{T_s} H(\alpha - \mathbf{1}^T \boldsymbol{f'}) \prod_{i=1}^{n-1} H(f_i) \tag{7}$$

where $H(f)$ is the Fourier transform of the impulse response $h(t)$, assumed bandlimited such that $H(f) = 0$ if $f \notin [-B/2; B/2]$. After having derived the nth order RD-CSMF, we focus on two particular cases, $n = 2$ and $n = 4$.

Example 1 (Second-order cyclostationarity). We obtain from (7):

$$S_s^{\alpha}(\boldsymbol{f'})_2 = \frac{R_{c,2}}{T_s} H(\alpha - f_1) H(f_1), \quad \alpha = \frac{p}{T_s},\ p \in \mathbb{Z}. \tag{8}$$

One remarks that

- if $\rho \leq 1$ (non-FTN case), then $1/T_s \leq B$ and there exists $f_1 \in \mathbb{R}$, $p \in \mathbb{Z}^*$ such that $S_s^{\alpha}(\boldsymbol{f'})_2 \neq 0$;
- if $\rho > 1$ (non-FTN case), then $1/T_s > B$ and $S_s^{\alpha}(\boldsymbol{f'})_2 = 0$ for any $f_1 \in \mathbb{R}$ and $p \in \mathbb{Z}^*$

In other words, the transmitted signal is not cyclostationary at the second order for FTN signals. This fact is crucial and makes it theoretically impossible to blindly estimate the symbol rate of FTN systems by means of a second order cyclostationary analysis of the received signals.

Example 2 (Fourth-order cyclostationarity). We obtain from (7):

$$S_s^{\alpha}(\boldsymbol{f'})_4 = \frac{R_{c,4}}{T_s} H(\alpha - (f_1 + f_2 + f_3)) H(f_1) H(f_2) H(f_3) \tag{9}$$

One remarks that independently of the value of ρ, there exists $\boldsymbol{f'}$, $p \in \mathbb{Z}^*$ such that

$$S_s^{\alpha}(\boldsymbol{f'})_4 \neq 0. \tag{10}$$

Therefore, a fourth-order analysis of the received signals allows blind symbol rate estimation for both non-FTN and FTN signals by means of an appropriate processing to be specified in the next Section.

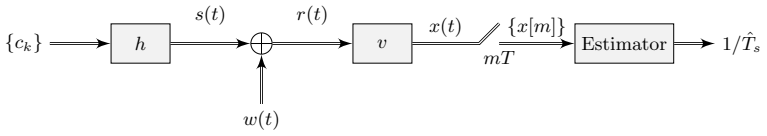

Fig. 1. Linear transmission system over a bandlimited AWGN channel.

2.3 Proposed estimator over the AWGN channel

System model is depicted in Figure 1. White noise with spectral density $2N_0$ is added to the linearly modulated signal:

$$r(t) = s(t) + w(t). \tag{11}$$

An ideal bandlimiting filter with frequency response $V(f) = 1/\sqrt{B}$ if $|f| \leq B/2$ and $V(f) = 0$ otherwise is then applied to the received signal so that

$$\begin{aligned} x(t) = (r * v)(t) &= \sum_{k=0}^{K-1} c_k (h * v)(t - kT_s) + (w * v)(t) \\ &= \sum_{k=0}^{K-1} c_k g(t - kT_s) + n(t) \end{aligned} \tag{12}$$

where $g(t) = (h*v)(t)$, $n(t) = (w*v)(t)$ and where K is the number of transmitted symbols. The signal is sampled at instants mT. We consider without loss of generality that T_s is a multiple of T:

$$x(mT) = \sum_{k=0}^{K-1} c_k g(mT - kT_s) + n(mT) \tag{13}$$

with $n(mT) \sim \mathcal{CN}(0, \sigma_n^2)$. Due to the finite impulse response of the transmission filter, we consider that $x(mT)$ can be truncated to M non-zero samples. At the receiver, an estimation of the RD-CTMF (5) is obtained by [17]

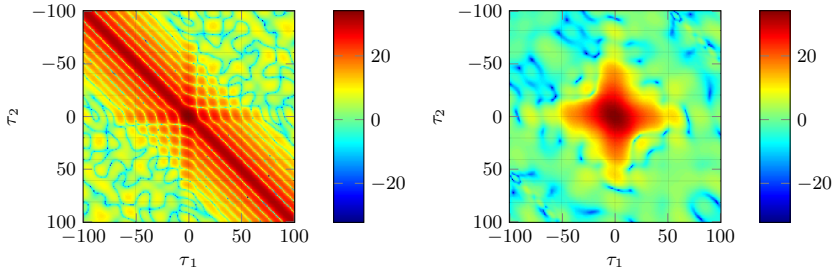

(a) $\alpha = 0$ (b) $\alpha = 1/T_s$

Fig. 2. Estimated fourth-order RD-CTMF, $10 \log \left(\hat{R}_s^{\alpha}(\boldsymbol{\tau}') \right)$, after $K = 60000$ transmitted symbols, $\rho = 1.2$, section $\tau_3 = 0$.

$$\hat{R}_x^{\alpha}(\boldsymbol{\tau}') = \frac{1}{T}\sum_{m=0}^{M-1} x^{(*)n}(mT)\prod_{i=1}^{n-1} x^{(*)i}(mT+\tau_i)e^{-j2\pi\frac{\alpha}{M}mT}. \tag{14}$$

where the transmitted signal is assumed to be nth order cycloergodic so that the expectation in (2) can be replaced by a time average [16]. The chosen blind symbol rate estimator based on [4] first computes (14) for all discrete delay vectors $\boldsymbol{\tau}'$ taken in $\mathcal{T} = \{-\Delta\tau/2, -\Delta\tau/2+1, \ldots, \Delta\tau/2\}^n$ with $\Delta\tau$ a positive integer. Secondly, the sum of squared absolute values from the previous step is maximized with respect to the (non-zero) cyclic frequency:

$$1/\hat{T}_s = \underset{\alpha\neq 0}{\operatorname{argmax}}\, \Psi(\alpha) \tag{15}$$

with

$$\Psi(\alpha) = \sum_{\boldsymbol{\tau}'\in\mathcal{T}} |\hat{R}_x^{\alpha}(\boldsymbol{\tau}')|^2. \tag{16}$$

In the following, the transmitted signal is built using a binary phase-shift keying (BPSK) constellation and a pulse shaping filter $h(t)$ chosen as a square-root-raised cosine (SRRC) with roll-off factor 0.2. Considering this excess bandwidth, the inter-symbol interference (ISI)-free reference is at $\rho = 0.83$. The oversampling factor is given by $T_s/T = 10$ and we set $T = 1$. Furthermore, (14) is implemented with a discrete Fourier transform so that $\alpha \in \mathcal{F}$ with

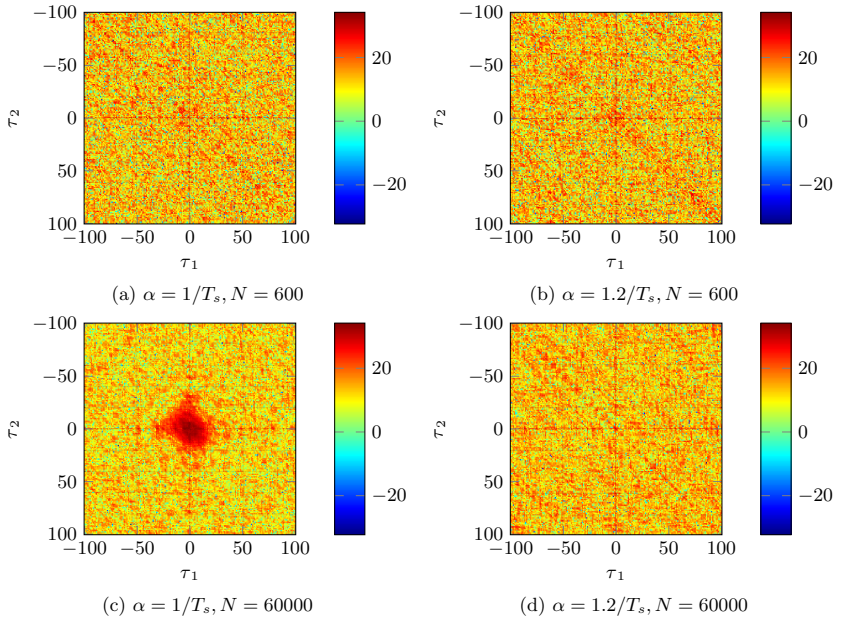

(a) $\alpha = 1/T_s, N = 600$ (b) $\alpha = 1.2/T_s, N = 600$

(c) $\alpha = 1/T_s, N = 60000$ (d) $\alpha = 1.2/T_s, N = 60000$

Fig. 3. Estimated fourth-order RD-CTMF, $10\log\left(\hat{R}_x^{\alpha}(\boldsymbol{\tau}')\right)$ for $E_b/N_0 = 5$ dB, $\rho = 1.2$, section $\tau_3 = 0$.

$\mathcal{F} = \{-1/2, -1/2 + 1/M, \ldots, 1/2 - 1/M\}$. Subsequent notation assumes that $0, -1/T_s, 1/T_s \in \mathcal{F}$, however approximate values do not change significantly the results as M gets large enough.

To illustrate the previous analysis, the empirical fourth-order RD-CTMF is depicted in Figure 2 in an FTN case ($\rho = 1.2$). A peak at $\alpha = 1/T_s$ confirms the ability to blindly estimate the symbol rate in the absence of noise. In Figure 3, the signal-noise-ratio is given by $E_b/N_0 = 5$ dB with E_b the energy per transmitted bit. Clearly, an observation of length $K = 600$ symbols is not sufficient to reveal cyclic features while $K = 60000$ seems sufficient.

We note that for $\alpha = 1/T_s$, the energy is distributed over a given delay span bounded by $\Delta\tau$. This observation will allow us in the following Section to configure the proposed ad-hoc symbol rate estimator.

3 Simulations

As stated before, the proposed estimator sums the available estimated RD-CTMFs over the delay span $\Delta\tau$ to produce a peak at the transmitted symbol rate. The estimated symbol rate corresponds to the cyclic frequency that maximizes $\Psi(\alpha)$. Figure 4 shows the aforementioned function to be maximized (excluding the continuous component $\alpha = 0$). Consequently, the estimator performance may be roughly measured through the dynamic range of $\Psi(\alpha)$, defined as the ratio between its value at the actual symbol rate and its mean:

$$R = \frac{\Psi(1/T_s)}{\bar{\Psi}(\alpha)} \tag{17}$$

where

$$\bar{\Psi}(\alpha) = \frac{1}{M-1} \sum_{\alpha \in \mathcal{F} \setminus \{0\}} \Psi(\alpha). \tag{18}$$

Figure 5 shows the dynamic range of the blind symbol rate estimator for different values of the maximum delay span $\Delta\tau$. As the span increases, the performance increases as well since the received white noise samples are averaged in time. In the following simulations, the time lag span is fixed to 10 samples.

Figure 6 shows the dynamic range of the blind symbol rate estimator for different system's densities. The dynamic range decreases with system's density and increases with E_b/N_0. After evaluating the dynamic range for various system densities, we observe that it is not linear in ρ and that density values above $\rho = 1.4$ yield an dynamic range close to 0 dB making impossible the symbol rate estimation with the values of E_b/N_0 and K considered so far.

The impact of the observed frame length on the dynamic range is shown in Figure 7 for $\rho = 1.2$. We show that for a given frame length, there is an E_b/N_0 threshold from which correct estimation is possible.

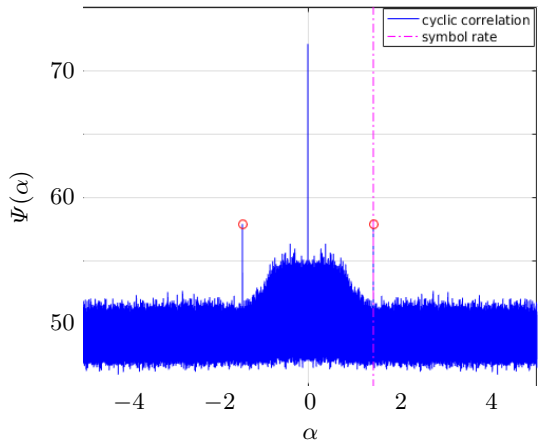

Fig. 4. Sum over $\tau_1, \ldots, \tau_3$ of the estimated fourth-order RD-CTMF, $E_s/N_0 = 5$ dB, $\rho = 1.2$, $K = 60000$ received symbols.

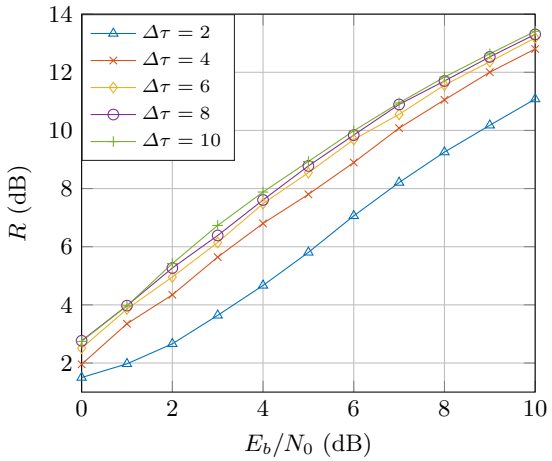

Fig. 5. Dynamic range of the symbol rate estimator for $\rho = 1.2$ and $K = 60000$.

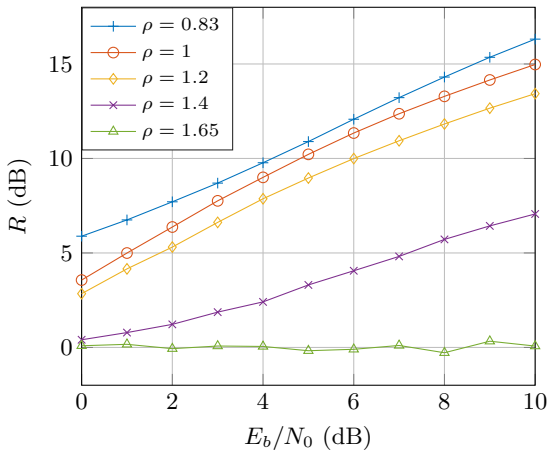

Fig. 6. Dynamic range of the symbol rate estimator for $K = 60000$.

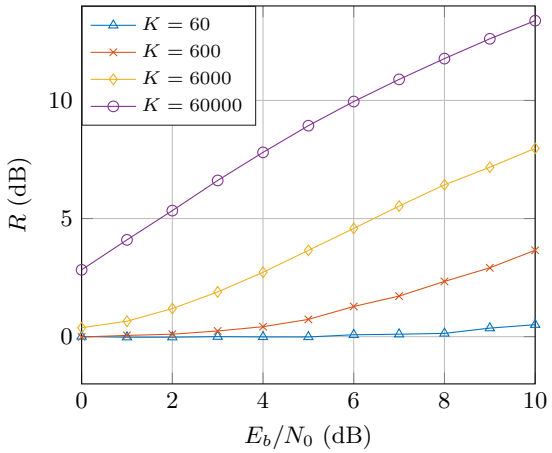

Fig. 7. Dynamic range of the symbol rate estimator for $\rho = 1.2$.

4 Conclusion

In this paper, we have addressed the problem of blind symbol rate estimation of FTN signals using fourth-order statistics. After showing that at least fourth-order statistics are required in the FTN case, we have evaluated by simulation the performance of an ad-hoc blind symbol rate estimator. Simulations show that performance is highly dependent on system's density, available frame length, and signal to noise ratio. In particular, the fourth-order symbol rate estimator shows good performance results for moderate system's densities (up to $\rho = 1.4$) and for high frames length (around $K = 60000$ received symbols). Future work should address the high density and short-length case by introducing other than fourth-order statistical signatures of the received signals. In addition to the dynamic range measurement, it would also be appropriate to extend the estimator performance evaluation to the calculation of its statistics. This work could also be extended to the case of general channel models.

Acknowledgements

The authors would like to thank Nghia Pham from Eutelsat S.A. and Thomas Gilles from ISAE-SUPAERO for their valuable comments and remarks. This work has been supported by the *Direction Générale de l'Armement* (DGA) under the CIFRE grant 10/2015/DGA.

Appendix: statistical moments for different conjugations

Below are listed all possible conjugation combinations and the resulting expectation term in the autocorrelation function in (2). We restrict our analysis up to fourth-order statistics of BPSK and quadrature phase-shift keying (QPSK) constellations. The expectation term has been defined as

$$R_{c,n} = \mathrm{E}\left\{c_{k_1}^{(*)1} \dots c_{k_n}^{(*)n}\right\}.$$

For a given constellation, we list below all possible combinations for the particular case $k_1 = k_2, \dots, k_n = k$:

$$R_{c,1} \in \left\{\mathrm{E}\left\{c_k\right\}, \mathrm{E}\left\{c_k^*\right\}\right\},$$
$$R_{c,2} \in \left\{\mathrm{E}\left\{c_k c_k\right\}, \mathrm{E}\left\{c_k^* c_k\right\}, \mathrm{E}\left\{c_k^* c_k^*\right\}\right\},$$
$$R_{c,3} \in \left\{\mathrm{E}\left\{c_k c_k c_k\right\}, \mathrm{E}\left\{c_k^* c_k c_k\right\}, \mathrm{E}\left\{c_k^* c_k^* c_k\right\} \mathrm{E}\left\{c_k^* c_k^* c_k^*\right\}\right\},$$
$$R_{c,4} \in \left\{\mathrm{E}\left\{c_k c_k c_k c_k\right\}, \mathrm{E}\left\{c_k^* c_k c_k c_k\right\}, \mathrm{E}\left\{c_k^* c_k^* c_k c_k\right\}, \mathrm{E}\left\{c_k^* c_k^* c_k^* c_k\right\}, \mathrm{E}\left\{c_k^* c_k^* c_k^* c_k^*\right\}\right\}.$$

For a BPSK constellation with $c_k \in \{1, -1\}$, we have $R_{c,1} = \{0, 0\}$, $R_{c,2} = \{1, 1, 1\}$, $R_{c,3} = \{0, 0, 0, 0\}$, $R_{c,4} = \{1, 1, 1, 1, 1\}$.

For a QPSK constellation with $c_k \in \{1 + j, 1 - j, -1 + j, -1 - j\}/\sqrt{2}$, we obtain $R_{c,1} = \{0, 0\}$, $R_{c,2} = \{0, 1, 0\}$, $R_{c,3} = \{0, 0, 0, 0\}$, $R_{c,4} = \{-1, 0, 1, 0, -1\}$.

Odd orders lead to all statistical moments being zero for zero-mean constellations. For the fourth-order statistical moments, additionally, the particular cases $k_1 = k_2, k_3 = k_4$ and $k_1 = k_3, k_2 = k_4$ are not zero and yield the same statistical moments presented before.

References

1. A. Abello, D. Roque, J.M. Freixe, and S. Mallier. Faster-than-nyquist signaling: on linear and non-linear reduced-complexity turbo equalization. *Analog Integrated Circuits and Signal Processing*, pages 1–10, 2017.
2. H. Arslan. *Cognitive radio, software defined radio, and adaptive wireless systems*, volume 10. Springer, 2007.
3. O. Christensen. *Frames and bases : an introductory course*. Applied and numerical harmonic analysis. Springer, Boston, Mass. Birkhäuser London, 2008. OHX.
4. P. Ciblat, P. Loubaton, E. Serpedin, and G. B. Giannakis. Asymptotic analysis of blind cyclic correlation-based symbol-rate estimators. *IEEE Transactions on Information Theory*, 48(7):1922–1934, Jul 2002.
5. C. Douillard, M. Jézéquel, C. Berrou, A. Picart, P. Didier, and A. Glavieux. Iterative correction of intersymbol interference: Turbo-equalization. *European Transactions on Telecommunications*, 6(5):507–511, 1995.
6. G Forney. Maximum-likelihood sequence estimation of digital sequences in the presence of intersymbol interference. *Information Theory, IEEE Transactions on*, 18(3):363–378, 1972.
7. W. A. Gardner and C. M. Spooner. The cumulant theory of cyclostationary time-series. i. foundation. *IEEE Transactions on Signal Processing*, 42(12):3387–3408, Dec 1994.
8. S. Haykin. Cognitive radio: brain-empowered wireless communications. *IEEE Journal on Selected Areas in Communications*, 23(2):201–220, Feb 2005.
9. P. Jallon and A. Chevreuil. Estimation of the symbol rate of linearly modulated sequences of symbols. *Signal Processing*, 88(8):1971 – 1979, 2008.
10. G. Maalouli and B.A. Bannister. Performance analysis of a MMSE turbo equalizer with LDPC in a FTN channel with application to digital video broadcast. In *Signals, Systems and Computers, 2014 48th Asilomar Conference on*, pages 1871–1875, Nov 2014.
11. J. E. Mazo. Faster-than-nyquist signaling. *Bell System Technical Journal*, 54(8):1451–1462, 1975.
12. M. McGuire and M. Sima. Discrete time faster-than-Nyquist signalling. In *Global Telecommunications Conference (GLOBECOM 2010), 2010 IEEE*, pages 1 –5, dec. 2010.
13. A. Napolitano. Cyclostationarity: New trends and applications. *Signal Processing*, 120:385 – 408, 2016.
14. N. Pham, J.B. Anderson, F. Rusek, J.M. Freixe, and A. Bonnaud. Exploring faster-than-Nyquist for satellite direct broadcasting. *AIAA International Communications Satellite Systems Conference*, pages 16–26, 2013.
15. A. Prlja and J. Anderson. Reduced-complexity receivers for strongly narrowband intersymbol interference introduced by faster-than-Nyquist signaling. *Communications, IEEE Transactions on*, 60(9):2591–2601, September 2012.

16. J. Renard, J. Verlant-Chenet, J.M. Dricot, P. De Doncker, and F. Horlin. Higher-order cyclostationarity detection for spectrum sensing. *EURASIP Journal on Wireless Communications and Networking*, 2010(1):721695, 2010.
17. C. M. Spooner and W. A. Gardner. The cumulant theory of cyclostationary time-series. ii. development and applications. *IEEE Transactions on Signal Processing*, 42(12):3409–3429, Dec 1994.
18. V. Turunen, M. Kosunen, A. Huttunen, S. Kallioinen, P. Ikonen, A. Parssinen, and J. Ryynanen. Implementation of cyclostationary feature detector for cognitive radios. In *2009 4th International Conference on Cognitive Radio Oriented Wireless Networks and Communications*, pages 1–4, June 2009.
19. M. Tüchler and A.C. Singer. Turbo equalization: An overview. *Information Theory, IEEE Transactions on*, 57(2):920–952, 2011.